International Journal of Power Electronics and Drive System (IJPEDS)
Vol. 17, No. 4, December 2026, pp. 2659∼2668
ISSN: 2088-8694, DOI: 10.11591/ijpeds.v17.i4.pp2659-2668

Design of an adaptive super-twisting sliding mode controller with extended state observer for robot manipulator trajectory tracking

Ahmed Bennaoui[1], Ameur Bennaoui[2], Hamza Sulimani[3], Idrees Nasser Alsolbi[4], Aissa Ameur[5]
[1]Institute of Sciences, University Center Aflou El Cherif Bouchoucha, Aflou, Algeria
[2]Computer Sciences, University of Constantine 2, Constantine, Algeria
[3]Department of Computer and Network Engineering, College of Computing, Umm Al-Qura University, Makkah, Saudi Arabia
[4]Department of Data Science, College of Computing, Umm Al-Qura University, Makkah, Saudi Arabia
[5]Faculty of Technology, University of Amar Telidji, Laghouat, Algeria

Article Info

Article history:

Received Mar 8, 2026
Revised Aug 18, 2026
Accepted Sep 17, 2026

Keywords:

Adaptive sliding mode control
Chattering mitigation
Disturbance estimation
Extended state observer
Robotic drive systems
Super-twisting algorithm

ABSTRACT

Sliding mode controllers often trade chattering suppression against rapid recovery from large initial tracking errors, yet the combined effect of severe initial offsets, high-bandwidth commands, and unmeasured disturbances remains insufficiently characterized within a single reproducible benchmark. This study compares classical SMC, fractional-order SMC (FOSMC), adaptive SMC, and a proposed adaptive super-twisting SMC with an extended state observer (AST-SMC+ESO) on a common two-degree-of-freedom planar manipulator under identical initial conditions, solver settings, and disturbances. The novelty of the proposed design is its combination of a leakage-regularized adaptive super-twisting gain with a third-order observer. Simulations show that AST-SMC+ESO achieves the lowest RMSE of the four controllers, 0.5958 rad and 0.5288 rad for joints 1 and 2, with peak torques of 260.03 N m and 86.48 N m. These peaks are below those of adaptive SMC and FOSMC but above those of classical SMC, which tracks far less accurately. FOSMC exhibits a persistent tracking offset and a torque peak exceeding 5.1 kN m, impractical for most actuators. AST-SMC+ESO thus offers a favorable compromise among robustness, tracking precision, and peak actuation demand for torque-limited drives such as collaborative robot joints. These results, obtained on an idealized rigid-body plant, motivate hardware-in-the-loop validation.

This is an open access article under the CC BY-SA license.

Corresponding Author:

Ahmed Bennaoui
Institute of Sciences, University Center Aflou El Cherif Bouchoucha
Aflou, 03001 Algeria
Email: a.bennaoui@cu-aflou.edu.dz

1. INTRODUCTION

Electromechanical drive manipulators in industrial automation, aerospace, and collaborative robotics must track demanding trajectories despite parameter drift and disturbances [1], [2], and their electric drive channels remain an active area of nonlinear control research [3]. Sliding mode control (SMC) offers robustness and finite-time convergence [4], but classical first-order designs chatter and degrade actuators [5]; this trade-off is most acute when a drive starts far from its commanded trajectory and must track a high-bandwidth reference without exceeding its torque limits. Recent work has pursued fractional-order smoothing, adaptive gain

tuning, and higher-order super-twisting schemes [6]-[10], including adaptive super-twisting observers with prescribed-time integral tracking [11], saturation-aware super-twisting laws [12], neural-network-observer backstepping designs [13], ESO-coupled data-driven adaptive SMC [14], and fault-tolerant/saturation-aware schemes for modular manipulators [15]. Yet most comparisons isolate one or two schemes at moderate initial error, omitting the switching-gain/observer-gain coupling that sets peak torque during large-offset recovery; the joint effect of severe initial offsets, high-bandwidth commands, and unmeasured disturbances on this tracking-versus-actuation trade-off remains uncharacterized within a single reproducible benchmark – the gap addressed here. This paper benchmarks a proposed adaptive super-twisting SMC with an extended state observer (AST-SMC+ESO) against classical SMC, fractional-order SMC (FOSMC), and adaptive SMC (ASMC) on a common two-DOF planar manipulator, initialized with large offsets and driven by high-bandwidth references, under identical conditions, solver settings, and disturbance patterns, grounded in established robot-modeling, sliding-mode, and observer-design foundations [16]-[21]. The contributions are threefold: i) a unified simulation framework for four SMC variants on the same model, ii) a standardized RMSE/MAE/IAE/ISE/torque evaluation, and iii) a torque-tracking trade-off analysis. Unlike prior designs that tune the switching gain and disturbance estimate separately [11], [13], [14], AST-SMC+ESO couples a leakage-regularized adaptive super-twisting gain with a third-order ESO so both are adjusted jointly from the same sliding-surface information – the mechanism behind its reduced peak torque without sacrificing tracking accuracy – with direct relevance to torque-limited drives such as collaborative robot joints and precision positioning stages [12], [15].

2. THE PROPOSED CONTROLLER DESIGN

2.1. Controller design and stability

This section presents the AST-SMC+ESO control law and its stability properties. The full manipulator model, excitation signals, and benchmarking protocol are provided in section 3. Classical SMC uses [4], [19].

$$u_i = K \tanh\left(\frac{s_i}{\delta}\right), \quad K = 25,\ \delta = 0.1. \tag{1}$$

FOSMC uses [6], [22].

$$s_i = \dot{e}_i + \alpha\, {}^{C}D_t^{1.5} e_i + \gamma |e_i|^{\beta} \operatorname{sign}(e_i), \tag{2}$$

With $(\alpha, \gamma, \beta) = (4, 9, 3)$ and $u_i = K_s \operatorname{sign}(s_i)$, $K_s = 10$. ${}^{C}D_t^{0.5} e_i$ is realized by an Oustaloup recursive approximation [6] of $s^{0.5}$ (band $[10^{-2}, 50]$ rad/s, $N = 5$; accurate to within 0.02 dB/3° at the system's operating frequencies); ${}^{C}D_t^{1.5} e_i$ is its exact time-derivative, using the known $\dot{e}_i$. Both filters start at their steady-state value for constant $e_i(0)$ (the Caputo derivative of a constant is zero), avoiding a nonphysical cold-start transient. ASMC uses [7], [20].

$$u_i = \hat{K}_i \tanh\left(\frac{s_i}{\delta}\right), \tag{3}$$

$$\dot{\hat{K}}_i = \gamma_{\text{adapt}} |s_i| - \eta_{\text{adapt}} \hat{K}_i, \tag{4}$$

With $\gamma_{\text{adapt}} = 20$ and $\eta_{\text{adapt}} = 0.01$; a projection stops the leakage term from driving $\hat{K}_i$ below the floor $K_{\min} = 0.1$. AST-SMC+ESO is [8]-[10], [21], [23].

$$u_i = \hat{k}_{1i} \sqrt{|s_i|} \operatorname{sign}(s_i) + z_i, \tag{5}$$

$$\dot{\hat{k}}_{1i} = \gamma_1 |s_i| - \eta(\hat{k}_{1i} - k_{\min}), \tag{6}$$

$$\dot{z}_i = k_{2i} \tanh\left(\frac{s_i}{0.05}\right), \quad k_{2i} = 0.5\hat{k}_{1i} + 0.5, \tag{7}$$

With $(\gamma_1, \eta, k_{\min}) = (8, 0.01, 0.1)$.

A third-order ESO is used in each channel [17], [24], with the innovation $y_i - x_{1i}$ clipped to ± 2 rad for numerical robustness:

$$\dot{x}_{1i} = x_{2i} + \beta_1 (y_i - x_{1i}), \tag{8}$$

$$\dot{x}_{2i} = x_{3i} + \beta_2(y_i - x_{1i}) + \ddot{q}_{\mathrm{nom},i}, \tag{9}$$

$$\dot{x}_{3i} = \beta_3(y_i - x_{1i}), \tag{10}$$

where $\hat{d}_i = x_{3i}$ (clipped to ± 30), $(\beta_1, \beta_2, \beta_3) = (8, 60, 120)$, and $\ddot{q}_{\mathrm{nom}} = B(q)^{-1}(\tau - C(q,\dot{q})\dot{q} - G(q))$ is the model-computed nominal joint acceleration used as the known-input term, rather than a constant $b_0 u_i$; computed from τ and the measured state through the B, C, G matrices of (14), it still requires only position and velocity feedback.

2.2. Conceptual comparison and implementation aspects

Relative to designs that adapt the switching gain and the disturbance/state observer through separate update laws [11], [13], coupling (6)–(7) with the ESO in (8)–(10) lets $\hat{k}_{1i}$ and $\hat{d}_i$ act jointly through (5). The ESO removes the slowly varying disturbance from the equivalent-control path, leaving the adaptive term to counter only the faster residual, which keeps peak torque lower than FOSMC while retaining finite-time convergence [8], [21]. Unlike the input-saturation-aware law of [12], saturation is not modeled explicitly; the leakage term $-\eta(\hat{k}_{1i} - k_{\min})$ bounds gain growth indirectly rather than through anti-windup. The control law and ESO need only position/velocity feedback plus the model-computed $\ddot{q}_{\mathrm{nom}}$, so no acceleration sensor is required [13]; the $\tanh(\cdot)$ smoothing in (7) and the continuity of $\sqrt{|s_i|}\,\mathrm{sign}(s_i)$ at $s_i = 0$ bound the switching discontinuity that would otherwise excite unmodeled dynamics [5], [15], though gains $(\beta_1, \beta_2, \beta_3, \gamma_1)$ would need re-tuning for a physical drive's bandwidth.

2.3. Stability statement

Assumption 1. Lumped uncertainties are bounded and piecewise differentiable, i.e., $|\Delta_i(t)| \le \bar{\Delta}_i$ and $|\dot{\Delta}_i(t)| \le \bar{\rho}_i$.

Theorem 1. Under bounded robot states and positive gains γ_1, η, and $k_{\min}$, AST-SMC+ESO drives s_i to a compact neighborhood of zero in finite time. The ultimate bound scales with disturbance-rate bounds and ESO estimation error.

Proof. For each joint, define $\xi_i = [|s_i|^{1/2}\,\mathrm{sign}(s_i), z_i]^\top$. Standard super-twisting analysis [8], [21] yields a positive-definite Lyapunov function V_i such that

$$\dot{V}_i \le -c_{1i}\|\xi_i\| + c_{2i}|\dot{\Delta}_i|. \tag{11}$$

The adaptive law increases $\hat{k}_{1i}$ when $|s_i|$ is large, while the leakage term prevents gain drift near the sliding manifold. Since $\dot{z}_i$ is bounded by the hyperbolic tangent term and $\hat{k}_{1i}$ remains bounded, all internal signals remain bounded. Summation over both joints establishes practical finite-time convergence of s_i.

3. METHOD

3.1. Research design and approach

This study uses a controller-benchmarking simulation design, holding the plant, disturbance, initial condition, reference profile, and solver settings fixed while varying only the control law, isolating the tracking-versus-actuation trade-off across four control structures and removing hardware-specific confounds (sensor noise, actuator bandwidth, communication delays) at the price of deferring them to future work.

3.2. Materials: system parameters and computational tools

The plant is a two-link planar manipulator with unit link length/mass ($L_1 = L_2 = 1$ m, $M_1 = M_2 = 1$ kg) and $g = 9.8$ m/s^2, setting the inertia matrix in (14), held identical across all controllers and joints. An unmeasured, acceleration-domain lumped disturbance.

$$d_1(t) = 0.6\sin(6.0t) + 0.2\sin(2.0t), \quad d_2(t) = 0.5\sin(5.0t) + 0.15\sin(1.5t), \tag{12}$$

The (12) is injected into the true joint accelerations of all four simulations identically and is not available to any controller; only AST-SMC+ESO carries an explicit ESO to estimate and compensate it, quantified in section 4. All simulations use Python 3, NumPy, SciPy (`scipy.integrate.solve_ivp`), pandas, and Matplotlib; no physical hardware, human subjects, or proprietary datasets were used.

3.3. Procedures: implementation steps

Pipeline: i) instantiate the plant model (section 3.4); ii) define the reference trajectories and large initial offset; iii) assemble each controller's closed-loop state equations, combining (16) with its switching law (state dimension 4 for SMC, 6 for ASMC, 14 for AST-SMC+ESO, 26 for FOSMC – two 11-state Oustaloup filters per (2); iv) integrate with adaptive-step `RK45` over $t \in [0, 5]$ s, tolerances $10^{-6}/10^{-8}$ [25]; v) resample onto a common 500-point grid and compute Table 1 statistics, exported to `performance_metrics.csv`. Applied identically to all four controllers.

3.4. Models, algorithms, and techniques

The two-DOF manipulator dynamics follow the Euler-Lagrange form [1], [2]:

$$B(q)\ddot{q} + C(q, \dot{q})\dot{q} + G(q) = \tau, \tag{13}$$

where $q = [\theta_1, \theta_2]^\top$ and $\boldsymbol{\tau} = [\tau_1, \tau_2]^\top$. The inertia matrix is

$$B(q) = \begin{bmatrix} 3 + 2\cos\theta_2 & 1 + \cos\theta_2 \\ 1 + \cos\theta_2 & 1 \end{bmatrix}. \tag{14}$$

Reference trajectories are $q_{d1}(t) = \sin(4.17t)$ and $q_{d2}(t) = 1.2\sin(5.11t)$. Initial conditions are $\theta_1(0) = -\pi$, $\theta_2(0) = \pi$, and $\dot{\theta}_1(0) = \dot{\theta}_2(0) = 0$; this offset of 2π and π rad, respectively, from the reference at $t = 0$ is deliberately severe so that the recovery transient, not only the steady-state tracking error, is exercised. Tracking errors are $e_i = q_i - q_{di}$, and the sliding surfaces are

$$s_i = \dot{e}_i + \lambda e_i, \quad \lambda = 15. \tag{15}$$

The equivalent control term is (16).

$$\tau_{eq} = B(q)(\ddot{q}_d - \lambda\dot{e}) + C(q, \dot{q})\dot{q} + G(q), \tag{16}$$

For SMC and ASMC, the switching action is applied directly in torque units, $\tau = \tau_{eq} - u$, with $u = [u_1, u_2]^\top$ given by (1)/(3). AST-SMC+ESO instead maps its correction through the inertia matrix, $\tau = \tau_{eq} - B(q)v$, $v_i = u_i + \hat{d}_i$ combining (5) with the ESO estimate of (10). FOSMC does not share this τ_{eq} structure: its reaching law needs additional terms compensating the time-derivative of $|e_i|^\beta \operatorname{sign}(e_i)$ in (2), implemented in the accompanying code but omitted here. Three limitations bound this model's scope: an idealized rigid-body arm without friction, backlash, or transmission flexibility, so torque figures characterize relative rather than absolute demand; a smooth, analytically known disturbance (12) rather than measured sensor noise; and nominal, exact inertia parameters, unlike a physical implementation facing uncertainty in M_1, M_2, L_1, L_2.

3.5. Validation and evaluation strategy

Each controller was evaluated per joint over the 5 s horizon on six criteria (Table 1): RMSE and MAE (average tracking accuracy), IAE and ISE (transient recovery speed), and mean/maximum torque (average/peak actuation demand), letting the torque-tracking trade-off in Section 4 be quantified rather than only described qualitatively. This study involves purely computational simulation, with no human or animal subjects, personal data, or physical experimentation, so no ethical approval was required.

4. RESULTS AND DISCUSSION

4.1. Presentation of results

Figures 1(a)–1(b) (see in Appendix) presents the joint-1 and joint-2 position responses of the four controllers against the desired trajectory. FOSMC, ASMC, and AST-SMC+ESO all recover from the large initial offset within roughly half a second, while classical SMC recovers markedly more slowly, remaining visibly offset through the first two reference cycles. Unlike ASMC and AST-SMC+ESO, which track the reference amplitude closely after recovery, FOSMC settles into a persistent steady-state overshoot, visible as amplitude peaks above the desired envelope, consistent with its higher steady-state error in Table 1. Figures 1(c)–1(d) (see in Appendix) reports the corresponding control torques τ_1, τ_2; the dominant feature is a brief FOSMC transient at $t = 0$, spiking to several kN m within the first fraction of a second before settling to a magnitude comparable with the other three controllers. Table 1 summarizes the resulting tracking and torque statistics for all four controllers on both joints. Figures 1(e)–1(f) (see in Appendix) shows AST-SMC+ESO's adaptive gain trajectories $\hat{k}_{1,1}, \hat{k}_{1,2}$ and its ESO disturbance estimates $\hat{d}_1, \hat{d}_2$.

Table 1. Tracking and control metrics over 5 s

Controller	Joint	RMSE	MAE	IAE	ISE	Mean $\lvert\tau\rvert$	Max $\lvert\tau\rvert$
SMC	1	1.5053	1.2525	6.2435	11.2541	48.9355	164.2936
SMC	2	0.8906	0.3623	1.7837	3.8748	23.0192	79.7338
FOSMC	1	0.7855	0.5942	2.9456	2.9926	62.6498	5124.8227
FOSMC	2	0.7812	0.5923	2.9358	2.9584	26.2733	637.3128
ASMC	1	0.7253	0.2007	0.9743	2.5370	61.9775	368.8410
ASMC	2	0.6150	0.1644	0.7924	1.7958	28.5930	224.7754
ASTSMC_ESO	1	0.5958	0.1421	0.6805	1.6794	65.1931	260.0267
ASTSMC_ESO	2	0.5288	0.1257	0.5985	1.3019	27.6331	86.4768

4.2. Analysis and interpretation

Table 1 shows AST-SMC+ESO attains the lowest RMSE of the four controllers on both joints (0.5958/0.5288 rad), ahead of ASMC (0.7253/0.6150), FOSMC (0.7855/0.7812), and SMC (1.5053/0.8906), while keeping its maximum torque to 260.03/86.48 N m, close to the SMC/ASMC peaks. FOSMC recovers as quickly as ASMC and AST-SMC+ESO (Figures 1(a)–1(b)), but its real fractional-order dynamics leave a persistent steady-state overshoot that raises its RMSE above theirs; its maximum torque reaches 5124.82/637.31 N m, one to two orders of magnitude above every other controller, traced by Figures 1(c)–1(d) to a brief, large switching transient at $t = 0$ rather than sustained effort. This is the torque-tracking trade-off the study set out to quantify: AST-SMC+ESO improves RMSE, MAE, IAE, and ISE relative to SMC, ASMC, and FOSMC alike, and relative to FOSMC specifically it does so while cutting peak torque by roughly an order of magnitude. Figure 1(e) shows $\hat{k}_{1,1}, \hat{k}_{1,2}$ rising sharply during recovery then settling once s_i is small, the adaptive law (6) acting as intended; Figure 1(f) shows the ESO estimates $\hat{d}_1, \hat{d}_2$ tracking the injected disturbance (12) after a $\sim$1 s transient, separating the disturbance from the large initial-offset transient.

4.3. Comparison with previous studies

These results agree with the chattering-versus-effort trade-off reported for high-gain and second-order sliding schemes [5], [18]: forcing fast recovery via a large reaching-law gain (FOSMC) costs large instantaneous torque, while smoother, gain-limited designs (SMC, ASMC, AST-SMC+ESO) trade some speed for bounded torque. FOSMC's persistent overshoot matches the fractional-order literature's observation [6], [22] that a fractional derivative's memory changes steady-state behavior, not just transient speed. The gap between AST-SMC+ESO and the more elaborate observer designs of [11], [13] which report comparable or better RMSE under more general uncertainty classes, suggests further gains from tightening the ESO/adaptive-law coupling beyond the leakage mechanism used here. Reported torques are demand, not what a saturated drive would deliver, consistent with [12], [15] being natural next steps; more broadly, this reinforces adaptive/higher-order SMC displacing fixed-gain first-order SMC in drive applications by reducing actuation demand without a proportional robustness loss [3].

4.4. Implications of findings

For practitioners, observer-assisted adaptive higher-order sliding control improves the tracking-versus-actuator-safety balance without the extreme torque margins a high-gain or fractional-order design would demand, directly relevant to torque-limited drives such as collaborative robot joints, where a several-kN m transient of the kind FOSMC exhibits (Figures 1(c)–1(d)) would exceed the actuator's rating regardless of tracking accuracy [5], [18], [19]. This also carries power-electronic implications: since the reference torque formed by (16) with (5), (7) is realized through an inner current loop, FOSMC's severe transient would demand far greater inverter/current-loop bandwidth and semiconductor current margin than the other controllers, risking switching losses, thermal stress, and EMI, whereas AST-SMC+ESO's smoother, order-of-magnitude-lower profile eases inverter sizing – a plausibility argument pending an explicit inverter model, but one extending equally to electric-vehicle traction joints and other power-stage-cost-sensitive drives. Future work should pursue hardware-in-the-loop validation, robustness under sensor noise, parameter drift, and actuator saturation, and an explicit current-loop/inverter model quantifying these bandwidth and EMI implications.

5. CONCLUSION

This work developed AST-SMC+ESO, coupling a leakage-regularized adaptive super-twisting gain with a third-order ESO, and benchmarked it against classical SMC, FOSMC, and ASMC on a common two-DOF manipulator under identical severe initial offsets, high-bandwidth references, and disturbances within a single reproducible benchmark. AST-SMC+ESO attained the lowest RMSE, MAE, IAE, and ISE of all four controllers on both joints, including FOSMC, while keeping its torque peaks an order of magnitude below FOSMC's. Its novelty is that the switching gain and disturbance estimate are adjusted jointly rather than independently, which kept peak torque low without the slow recovery of classical SMC, a benefit that also extends to the inverter and current-loop hardware that would realize the commanded torque.

Three limitations bound this study: an idealized rigid-body arm without friction, backlash, or transmission flexibility; a disturbance that, though applied identically to all controllers, is a smooth analytical signal rather than measured noise; and gains tuned in simulation, not claimed to transfer without re-tuning to a physical actuator – so reported torques are a comparative demand, not an actuator-sizing specification. Future work will pursue hardware-in-the-loop validation, actuator-saturation-aware redesign, and robustness testing under sensor noise, parameter drift, and unmodeled friction.

FUNDING INFORMATION

This research work was funded by Umm Al-Qura University, Saudi Arabia, under grant number 26UQU4320283GSSR03.

AUTHOR CONTRIBUTIONS STATEMENT

This journal uses the Contributor Roles Taxonomy (CRediT) to recognize individual author contributions, reduce authorship disputes, and facilitate collaboration.

Name of Author	C	M	So	Va	Fo	I	R	D	O	E	Vi	Su	P	Fu
Ahmed Bennaoui	✓	✓			✓				✓					
Ameur Bennaoui			✓			✓		✓		✓				
Hamza Sulimani		✓	✓	✓						✓				✓
Idrees Nasser Alsolbi				✓	✓					✓				✓
Aissa Ameur	✓	✓			✓	✓				✓		✓	✓	

C : **C**onceptualization
M : **M**ethodology
So : **So**ftware
Va : **Va**lidation
Fo : **Fo**rmal Analysis
I : **I**nvestigation
R : **R**esources
D : **D**ata Curation
O : Writing - **O**riginal Draft
E : Writing - Review & **E**diting
Vi : **Vi**sualization
Su : **Su**pervision
P : **P**roject Administration
Fu : **Fu**nding Acquisition

CONFLICT OF INTEREST STATEMENT

The authors declare that they have no known competing financial or non-financial interests.

DATA AVAILABILITY

The data supporting the findings of this study are available from the corresponding author upon reasonable request. Core generated outputs include `performance_metrics.csv` and the associated published figures.

REFERENCES

[1] M. W. Spong, S. Hutchinson, and M. Vidyasagar, *Robot modeling and control*. John Wiley & Sons, 2006.
[2] J. J. Craig, *Introduction to robotics: mechanics and control*, 3rd ed. Pearson Prentice Hall, 2005.
[3] A. K. Junejo, W. Xu, M. A. Abido, M. Hamouda, J. R. Perez, and Y. Tang, "Recent developments in sliding mode control for electric drives: performance assessment, and comparative evaluation with conventional techniques," *IEEE Transactions on Power Electronics*, pp. 1–21, 2026, doi: 10.1109/TPEL.2026.3662470.
[4] V. I. Utkin, *Sliding modes in control and optimization*. Springer, 1992.

[5] X. Yu and O. Kaynak, "Sliding-mode control with soft computing: a survey," *IEEE Transactions on Industrial Electronics*, vol. 56, no. 9, pp. 3275–3285, Sep. 2009, doi: 10.1109/TIE.2009.2027531.
[6] C. A. Monje, Y. Chen, B. M. Vinagre, D. Xue, and V. Feliu, *Fractional-order systems and controls*. in Advances in Industrial Control. London: Springer London, 2010, doi: 10.1007/978-1-84996-335-0.
[7] F. Plestan, Y. Shtessel, V. Brégeault, and A. Poznyak, "New methodologies for adaptive sliding mode control," *International Journal of Control*, vol. 83, no. 9, pp. 1907–1919, Sep. 2010, doi: 10.1080/00207179.2010.501385.
[8] J. A. Moreno and M. Osorio, "Strict lyapunov functions for the super-twisting algorithm," *IEEE Transactions on Automatic Control*, vol. 57, no. 4, pp. 1035–1040, Apr. 2012, doi: 10.1109/TAC.2012.2186179.
[9] Y. Shtessel, M. Taleb, and F. Plestan, "A novel adaptive-gain supertwisting sliding mode controller: methodology and application," *Automatica*, vol. 48, no. 5, pp. 759–769, May 2012, doi: 10.1016/j.automatica.2012.02.024.
[10] A. Chalanga, S. Kamal, L. M. Fridman, B. Bandyopadhyay, and J. A. Moreno, "Implementation of super-twisting control: super-twisting and higher order sliding-mode observer-based approaches," *IEEE Transactions on Industrial Electronics*, vol. 63, no. 6, pp. 3677–3685, Jun. 2016, doi: 10.1109/TIE.2016.2523913.
[11] H. Shen, T. Song, L. Fang, H. Wang, and Y. Zhang, "Adaptive super twisting observer-based prescribed time integral sliding mode tracking control of uncertain robotic manipulators," *International Journal of Adaptive Control and Signal Processing*, vol. 38, no. 7, pp. 2588–2616, 2024, doi: 10.1002/acs.3824.
[12] C. Jing, H. Zhang, Y. Liu, and J. Zhang, "Adaptive super-twisting sliding mode control for robot manipulators with input saturation," *Sensors*, vol. 24, no. 9, 2024, doi: 10.3390/s24092783.
[13] R. D. Xi, T. N. Ma, X. Xiao, and Z. X. Yang, "Design and implementation of an adaptive neural network observer–based backstepping sliding mode controller for robot manipulators," *Transactions of the Institute of Measurement and Control*, vol. 46, no. 6, pp. 1093–1104, 2024, doi: 10.1177/01423312231190169.
[14] H. Khan, S. A. Khan, M. C. Lee, U. Ghafoor, F. Gillani, and U. H. Shah, "DDPG-based adaptive sliding mode control with extended state observer for multibody robot systems," *Robotics*, vol. 12, no. 6, Nov. 2023, doi: 10.3390/robotics12060161.
[15] Z. Lu, Y. Li, X. Fan, Q. Wang, and Y. Li, "Decentralized fault-tolerant control of modular robot manipulators with actuator saturation: neural adaptive integral terminal sliding mode-based control approach," *Complex & Intelligent Systems*, vol. 9, no. 6, pp. 7495–7510, Dec. 2023, doi: 10.1007/s40747-023-01142-z.
[16] J.-J. E. Slotine and W. Li, *Applied nonlinear control*. Englewood Cliffs, NJ. Prentice hall, 1991.
[17] Y. Shtessel, C. Edwards, L. Fridman, and A. Levant, "Sliding mode control and observation," *Sliding Mode Control and Observation*, pp. 1–356, 2014, doi: 10.1007/978-0-8176-4893-0.
[18] I. Boiko, L. Fridman, A. Pisano, and E. Usai, "Analysis of chattering in systems with second-order sliding modes," *IEEE Transactions on Automatic Control*, vol. 52, no. 11, pp. 2085–2102, 2007, doi: 10.1109/TAC.2007.908319.
[19] H. Lee, V. I. Utkin, and A. Malinin, "Chattering reduction using multiphase sliding mode control," *International Journal of Control*, vol. 82, no. 9, pp. 1720–1737, 2009, doi: 10.1080/00207170902725607.
[20] V. I. Utkin and A. S. Poznyak, "Adaptive sliding mode control with application to super-twist algorithm: equivalent control method," *Automatica*, vol. 49, no. 1, pp. 39–47, 2013, doi: 10.1016/j.automatica.2012.09.008.
[21] A. Levant, "Higher-order sliding modes, differentiation and output-feedback control," *International Journal of Control*, vol. 76, no. 9–10, pp. 924–941, Jan. 2003, doi: 10.1080/0020717031000099029.
[22] S. Ahmed, A. T. Azar, and M. Tounsi, "Design of adaptive fractional-order fixed-time sliding mode control for robotic manipulators," *Entropy*, vol. 24, no. 12, 2022, doi: 10.3390/e24121838.
[23] K. Kumari, A. Chalanga, and B. Bandyopadhyay, "Implementation of super-twisting control on higher order perturbed integrator system using higher order sliding mode observer," *IFAC-PapersOnLine*, vol. 49, no. 18, pp. 873–878, 2016, doi: 10.1016/j.ifacol.2016.10.276.
[24] J. Han, "From pid to active disturbance rejection control," *IEEE Transactions on Industrial Electronics*, vol. 56, no. 3, pp. 900–906, Mar. 2009, doi: 10.1109/TIE.2008.2011621.
[25] E. Hairer, S. P. Nørsett, and G. Wanner, *Solving ordinary differential equations i: nonstiff problems*, 2nd ed. Berlin, Germany: Springer, 1993.

APPENDIX

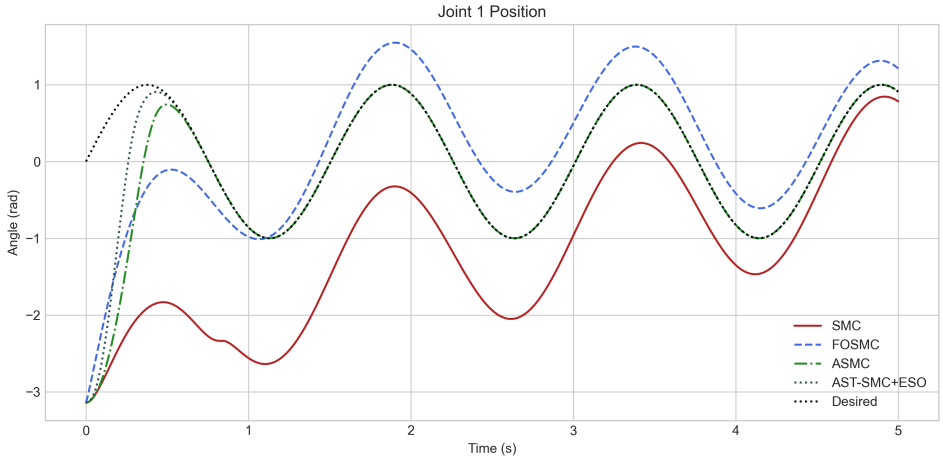

(a)

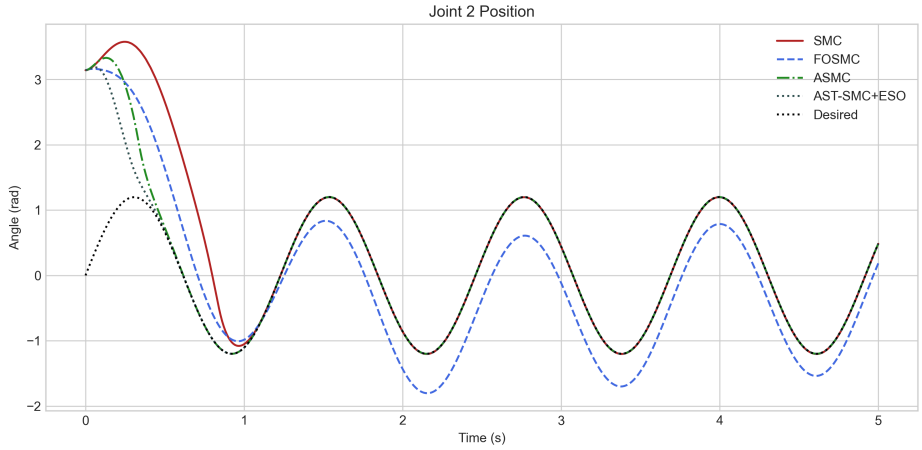

(b)

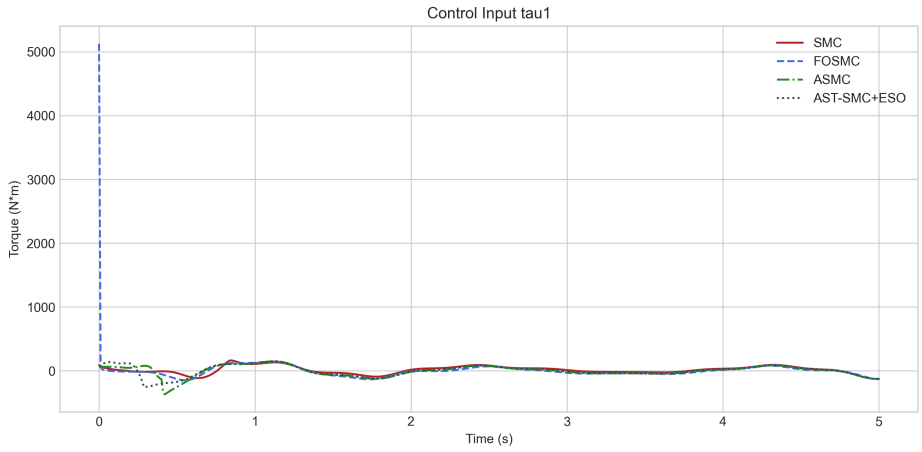

(c)

Figure 1. Comparison of SMC, FOSMC, ASMC, and AST-SMC+ESO over $t \in [0, 5]$ s: (a) joint 1 position tracking, (b) joint 2 position tracking, and (c) joint 1 torque

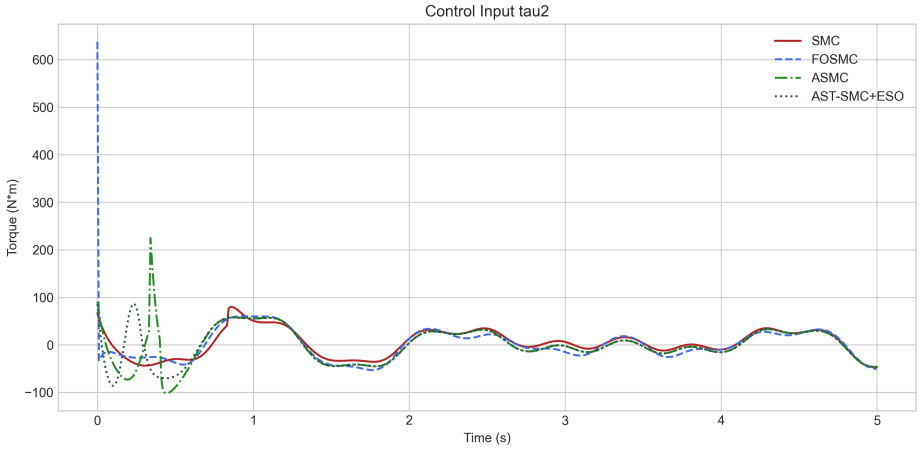

(d)

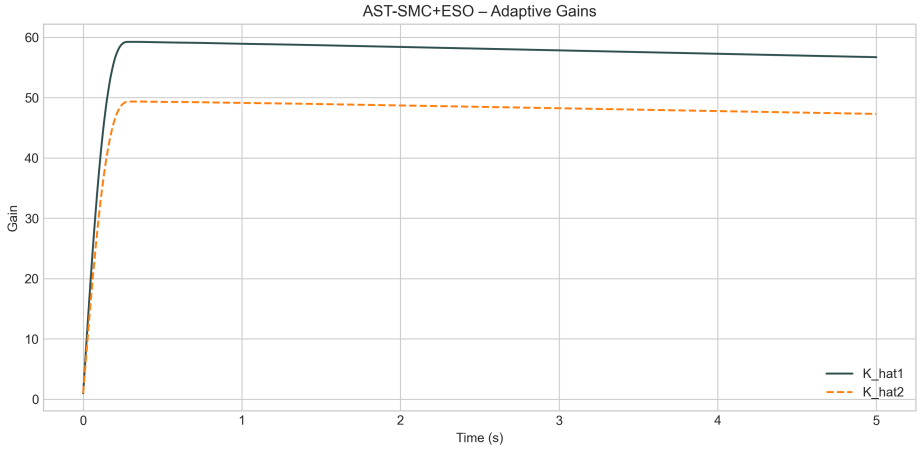

(e)

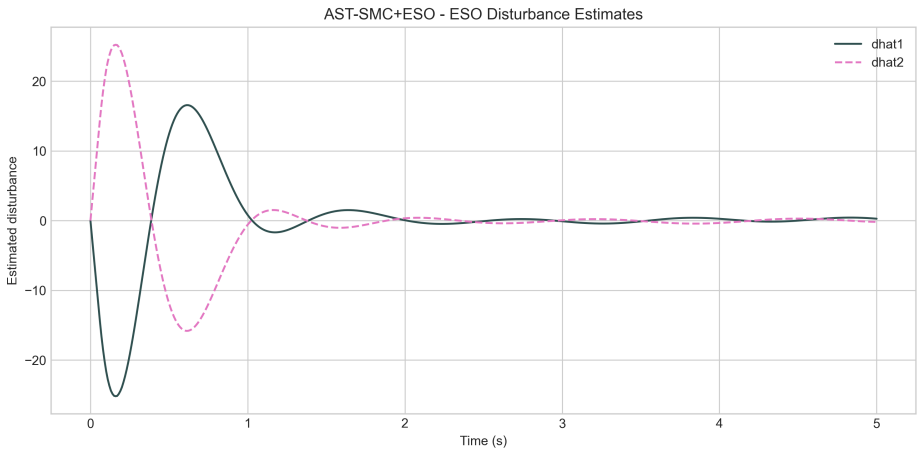

(f)

Figure 1. Comparison of SMC, FOSMC, ASMC, and AST-SMC+ESO over $t \in [0, 5]$ s: (d) joint 2 torque, (e) AST-SMC+ESO's adaptive gains $\hat{k}_{1,1}, \hat{k}_{1,2}$, and (f) its ESO disturbance estimates $\hat{d}_1, \hat{d}_2$ (continued)

BIOGRAPHIES OF AUTHORS



Ahmed Bennaoui received the Ph.D. in electrical engineering (intelligent control and automation) from the University of Amar Telidji, Laghouat, Algeria, in 2024. His research interests include nonlinear dynamics, fuzzy logic control, power system control, and optimization. He can be contacted at email: a.bennaoui@cu-aflou.edu.dz.



Ameur Bennaoui received his engineering degree in telecommunications and his Master of Science degree in information and communication technologies from INTTIC, Oran, Algeria, in 2006 and 2010, respectively. He received his Doctor of Philosophy degree in computer science in 2026. He is a lecturer in the Department of Computer Science at the University of Constantine 2, Algeria. His research interests include vehicular ad hoc networks, artificial intelligence, machine learning, network security, and intelligent transportation systems. He contributed to the Python implementation, data curation, and manuscript review. He can be contacted at email: ameur.bennaoui@univ-constantine2.dz.



Hamza Sulimani is an assistant professor in the Department of Computer and Network Engineering, College of Computing, Umm Al-Qura University, Makkah, Saudi Arabia. He received his Bachelor of Science degree in electrical and computer engineering from Umm Al-Qura University in 2000, his Master of Science degree in electrical and computer engineering from King Abdulaziz University in 2010, and his Doctor of Philosophy degree in information technology from the University of Technology Sydney, Australia, in 2024. His research interests include computer network architectures, cybersecurity, fog computing for Internet of Things (IoT) protection, and machine learning applications in network traffic analysis. He can be contacted at email: hhhsulimani@uqu.edu.sa.



Idrees Nasser Alsolbi received his Doctor of Philosophy degree in big data from the University of Technology Sydney, Australia, in 2023. He is an assistant professor and the Head of the Department of Data Science at the College of Computing, Umm Al-Qura University, Saudi Arabia. His research interests include big data analytics, machine learning, edge computing, and artificial intelligence-based decision support systems. He can be contacted at email: insolbi@uqu.edu.sa.



Aissa Ameur received his Doctor of Philosophy degree in electrical engineering from Batna University, Algeria, in 2012. He is an assistant professor at the University of Amar Telidji, Laghouat, Algeria, and a researcher at the LeDMaScD Laboratory. His research interests include electrical machine modeling, drive control, fault diagnosis, and renewable energy systems. He can be contacted at email: a.ameur@lagh-univ.dz.